Polarization analyses of readout signals by a solid immersion lens in phase change recording material

Chung-Hao Tien
Yin-Chieh Lai
Han-Ping David Shieh
National Chiao Tung University
Institute of Electro-Optical Engineering
Hsin-Chu, 30010 Taiwan
E-mail: chtien.eo86g@nctu.edu.tw

Abstract. Comprehensive analyses based on the rigorous vector diffraction theory were used to simulate the polarized readout signals using a solid immersion lens (SIL) in reading phase change (PC) disks. For an *x*-polarized incident beam, the signal contrast in *x* and *y* polarization was a different function of air gap between the bottom surface of the SIL and recording medium. Compared with conventional nonpolarized detection schemes for PC media, the *x*-polarized contrast is a factor 1.0 to 1.35 higher at different air gaps, at a small cost of total intensity loss. [DOI: 10.1117/1.1399284]

Subject terms: solid immersion lens (SIL); near-field recording; numerical aperture; polarization; vector diffraction.

Paper PT-003 received Nov. 30, 2000; revised manuscript received Apr. 10, 2001; accepted for publication Apr. 10, 2001.

1 Introduction

The area density of optical data storage is determined by the size of the focusing spot, which is limited by diffraction to approximately $0.5\,\lambda_0$/numerical aperture (NA), where λ_0 is the wavelength of the laser and NA is the numerical aperture of the focusing lens. Fortunately, the diffraction limit can be circumvented by the use of near-field optics. In 1984 Pohl, Denk, and Lanz[1] demonstrated a near-field optical microscope using a glass rod tapered down to a small pinhole and covered with a deposited metal film. To obtain a resolution comparable to the diameter of the pinhole, the pinhole must be placed within a distance from the sample comparable to the pinhole size. Betzig et al.[2] used a taped fiber with a pinhole at the end to demonstrate a resolution of 60 nm with a 488-nm light source. Hosaka et al.[3] utilized near-field optics to record in phase change (PC) media, and achieved a minimum record bit of 60 nm with a 785-nm laser. One major issue in using these near-field optical taped fiber techniques was the high transmission loss of the light, which resulted in a low data rate. A different method with solid immersion lens (SIL) proposed by Kino et al.[4,5] provided a real-time scanning image directly, required no mechanical scanning, had a better light budget, and could be easily added onto an existing optical data storage system. Thus, the SIL-based[6–8] optical system was supposed to be more feasible than other near-field techniques in real-time optical information storage applications.

By focusing light from an objective onto the lower surface of a high refractive index lens without another refraction, as shown in Fig. 1, the wavelength of light is shrunk by a factor *n*, where *n* is the refractive index of the lens. Hence the resolution is expected to improve by a factor *n*. Based on a vector diffraction theory using plane-wave expansion, the spectra within the critical angle of the SIL-air interface diffract like a focus wave with NA = 1.0, while the other parts decay exponentially away from the bottom of the SIL. When the SIL is positioned closely enough to the disk, the optical tunneling effect of the evanescent wave results in increasing the effective NA_{eff} above the theoretical upper limit of 1.0 in the air.[9,10]

For SIL systems with $NA_{eff} > 1.0$, the flying height of the coupling element above the disk critically affects the readout performance. We investigate the dependence of the signal contrast on gap width less than the wavelength of the incident light. Furthermore, the phase and amplitude changes of the waves passing through the air gap depend on their polarizations. Scalar theory is, therefore, inadequate. Instead, a more rigorous vector field theory is employed to analyze numerically polarization effects on the readout signal with the SIL-based system in reading phase change media.

2 System Layout

We adopt a linearly *x*-polarized Gaussian beam with a 1/e amplitude radius of $r_0 = \mathrm{RA}$ (RA is the objective radius) for 0.6- and 0.8-NA objective lens with SIL ($n = 2.0$), resulting in an effective $NA_{eff} = 1.1$ and 1.48, respectively. The reflected beam is collimated, separated into the *x*- and *y*-polarized electric fields by a polarizing beamsplitter (PBS) and then detected, denoted by S_1 and S_2, respectively, as shown in Fig. 1. The disk structure is optimized for maximum signal contrast of the Gaussian incident beam.[11] The thin film is assumed to be homogeneous; thus the mark patterns are not included in the analyses. Here the signal contrast is defined as $V_i = (S_{Xi} - S_{Ai})/(S_{Xi} + S_{Ai})$ ($i = 1, 2$: *x*, *y* polarization, respectively), where S_X and S_A are

This paper is a revision of a paper presented at the SPIE conference on Optical Storage and Optical Information Processing, July 2000, Taipei, Taiwan. The paper presented there appears (unrefereed) in SPIE Proceedings Vol. 4081.

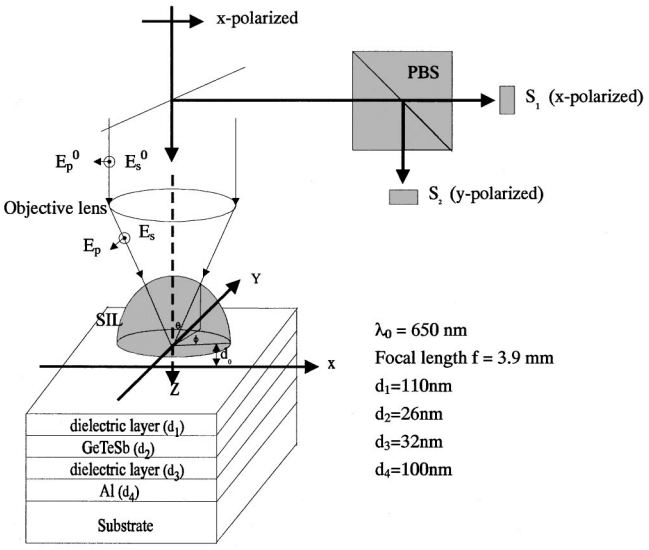

Fig. 1 Schematics of an SIL-based optical system and disk structure.

the reflected intensity due to the crystalline and amorphous states, respectively.

3 Simulation Methods

Our approach to vector diffraction is based on Mansuripur[12,13] and Kino et al.[6] A wavefront is decomposed into a set of plane waves that propagate independently through the SIL system. Then each plane wave propagation in θ and ϕ directions is associated with its two orthogonal electric fields at the input pupil plane, E_p^0 and E_s^0, which are parallel and perpendicular to the plane of incidence, respectively, as shown in Fig. 1. After being reflected from the layered media, the two independent electric fields, E_p and E_s, can be written as follows[6,14]:

$$\begin{bmatrix} E_p \\ E_s \end{bmatrix} = \begin{bmatrix} r_{pp} & r_{ps} \\ r_{sp} & r_{ss} \end{bmatrix} \begin{bmatrix} E_p^0 \\ E_s^0 \end{bmatrix}, \tag{1}$$

$$\theta = \tan^{-1}\left(\frac{(E_x^2 + E_y^2)^{1/2}}{E_z} \right), \tag{2}$$

$$\phi = \tan^{-1}\left(\frac{E_y}{E_x} \right), \tag{3}$$

where the diagonal terms, r_{pp} and r_{ss}, are complex reflection coefficients for *p*- and *s*-polarized components, and r_{ps} and r_{sp} are cross terms between *p*- and *s*-polarized components, which are zero in homogeneous and isotropic media such as PC. After coordinate transformation, the polarization of a refracted beam can be expressed in terms of the incident beams in Cartesian coordinates:

$$\begin{bmatrix} E_x \\ E_y \\ E_z \end{bmatrix} = \begin{bmatrix} \psi_{xx} \psi_{xy} \\ \psi_{yx} \psi_{yy} \\ \psi_{zx} \psi_{zy} \end{bmatrix} \begin{bmatrix} E_x^0 \\ E_y^0 \end{bmatrix}, \tag{4}$$

where

$$\begin{aligned}
\psi_{xx} &= \tfrac{1}{2}[(r_{ss} + r_{pp}\cos\theta) - (r_{ss} - r_{pp}\cos\theta)\cos 2\phi \\
&\quad - (r_{sp} + r_{ps}\cos\theta)\sin 2\phi] \\
\psi_{xy} &= \tfrac{1}{2}[(r_{sp} - r_{ps}\cos\theta) - (r_{sp} + r_{ps}\cos\theta)\cos 2\phi \\
&\quad + (r_{ss} - r_{pp}\cos\theta)\sin 2\phi] \\
\psi_{yx} &= \tfrac{1}{2}[(r_{sp} - r_{ps}\cos\theta) + (r_{sp} + r_{ps}\cos\theta)\cos 2\phi \\
&\quad - (r_{ss} - r_{pp}\cos\theta)\sin 2\phi] \\
\psi_{yy} &= \tfrac{1}{2}[(r_{ss} + r_{pp}\cos\theta) + (r_{ss} - r_{pp}\cos\theta)\cos 2\phi \\
&\quad + (r_{sp} + r_{ps}\cos\theta)\sin 2\phi] \\
\psi_{zx} &= (r_{pp}\cos\phi - r_{ps}\sin\phi)\sin\theta \\
\psi_{zy} &= (r_{ps}\cos\phi + r_{pp}\sin\phi)\sin\theta.
\end{aligned} \tag{5}$$

At a focal length from the bottom of the SIL along the *z* axis, the electric field distribution at the output pupil is obtained by superimposing each plane wave, taking into account different propagation paths and polarization vectors. The integral of the overall electric field can be computed efficiently by the fast-Fourier-transform (FFT) algorithm.

4 Results and Discussions

The variation of the field distribution at the output pupil is due to the vectorial nature of interaction between the incident beam and multilayer stacks. In the calculation, the refractive indices of the PC media are $4.6+4.2i$ for the crystalline state and $4.2+1.9i$ for the amorphous state at $\lambda_0 = 650$ nm. The reflection coefficients r_{pp}, r_{ss}, calculated by a 2×2 thin-film matrix formula, are strong functions of the angle of incidence θ, the polarization of incident wave, and the air gap d_0, as shown in Fig. 2. Note that the marginal incident angle of NA=0.6 objective is approximately 37 deg. At 0-nm gap width, $|r_{ss}|$ and $|r_{pp}|$ are similar to conventional reflectance on the surface of four-layer PC media, shown in Fig. 1. When $d_0 = 100$ nm, $|r_{ss}|$ and $|r_{pp}|$ of the rays in an evanescent mode (above critical angle $\theta_c = 30$ deg) are comparable with those of small incident angles. As the air gap widens up to 300 nm, $|r_{ss}|$ and $|r_{pp}|$ of the rays in evanescent mode are drastically increased. Thus, field distributions obtained by superimposing each reflected plane wave with individual $|r_{ss}|$ and $|r_{pp}|$ [i.e., the integration of $|E_x|^2 + |E_y|^2$ in Eq. (5)] at the output pupil are not only variously distributed but also varied with gap width. Reflected intensity distributions of crystalline (i_X) and amorphous state (i_A) in *x* polarization at the output pupil of $NA_{eff} = 1.1$ system are shown in Figs. 3(a) and 3(b), respectively, with gap width of 100 and 300 nm. At 100-nm gap width, the bright center region indicates an area of high reflectance with small incident angles on the four-layered sandwiched structure. The rim of the dark oval-shape region is due to the rays in *s* and *p* waves at higher incident angles having different reflectances, thus inducing an unsymmetrical distribution in Cartesian coor-

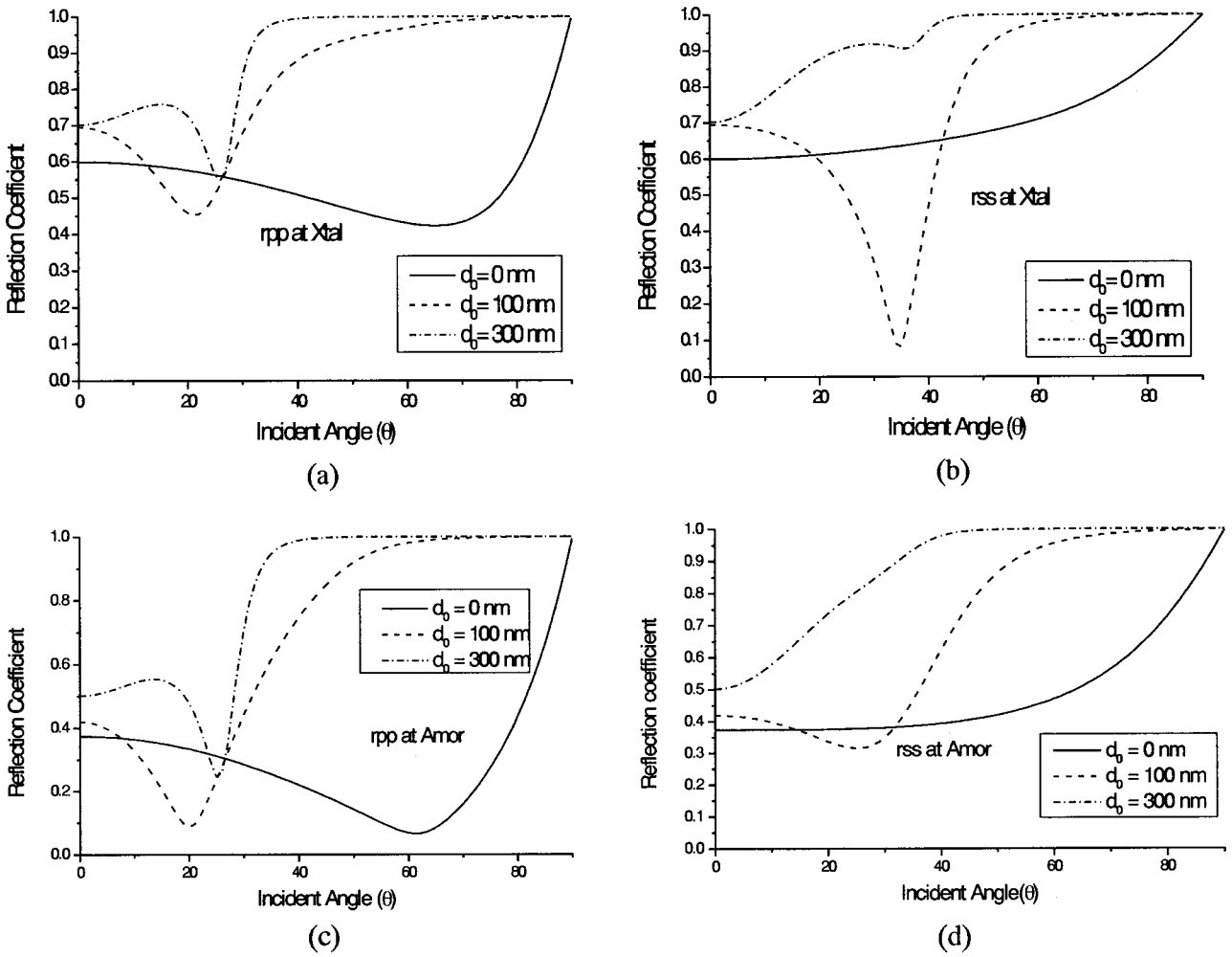

Fig. 2 Amplitude reflection coefficients are functions of the angle of incidence θ, the incident polarization (*s* and *p* wave), and the structure of the thin-film layers. (a) r_{pp}, (b) r_{ss} for the crystalline state, (c) r_{pp}, and (d) r_{ss} for the amorphous state of the recording layer at different air gap widths 0, 100, and 300 nm, respectively.

dinates. When the gap width increases up to 300 nm, the enlarged bright center region implies the reduction of interaction between incident beam and recording medium within a given incident spectrum. There is also a gradually bright ring around the margins, resulted from the decrease of evanescent coupling with an increase of incident angle. The phenomenon is more apparent for higher NA systems. Moreover, the contrast distributions $(i_X - i_A)/(i_X + i_A)$ in *x* polarization are shown in Fig. 3(c). Bipolar distribution in *x* polarization displays two minimum regions along the *y* direction, around the area defined by $i_x < i_A$. In contrast, two maximum regions along the *x* direction show $i_x > i_A$. Milster et al.[15] used a pupil-plane filtering to block the negative distribution to improve signal contrast.

The *y*-polarized quadruple symmetric distribution is sizable for high NA systems such as the SIL-based system. Now with $NA_{eff}=1.1$, reflected intensity distributions of crystalline (i_X) and amorphous state (i_A) in *y* polarization at the output pupil are shown in Figs. 4(a) and 4(b), respectively, at gap widths 100 and 300 nm. As the gap width increases, the bright quadruple region is toward the margin of aperture and becomes stronger, indicating that rays with large incident angles are reflected increasingly. Compared with *x* polarization, the contrast distributions in *y* polarization are centrally symmetrical as shown in Fig. 4(c). Similarly, the contrast decreases with the increase of gap width.

In the preceding discussion, we show that the reflected field and contrast distributions in *x* and *y* polarizations were different. Moreover, the detected signal S_X and S_A, and integration of i_x and i_A over the pupil contributed from the *x* and *y* components are also different. A numerical analysis for the case of 100-nm gap width is used to further examine this discrepancy. The positive or negative signal contributions are determined by whether $S_x > S_A$ or $S_x < S_A$, respectively. After integration of i_X and i_A across the pupil, the reflectance in *x* polarization of crystalline (S_{X1}) and amorphous state (S_{A1}) is 29 and 9.4%, respectively. The reflectance in *y* polarization of crystalline (S_{X2}) and amorphous state (S_{A2}) is 4.3 and 2.4%, respectively. The signal contrast of *x* (V_1) and *y* polarization (V_2) is 0.511 and 0.287, respectively. Therefore, both reflected intensity and contrast from the original incident polarized light (*x* polarized) are

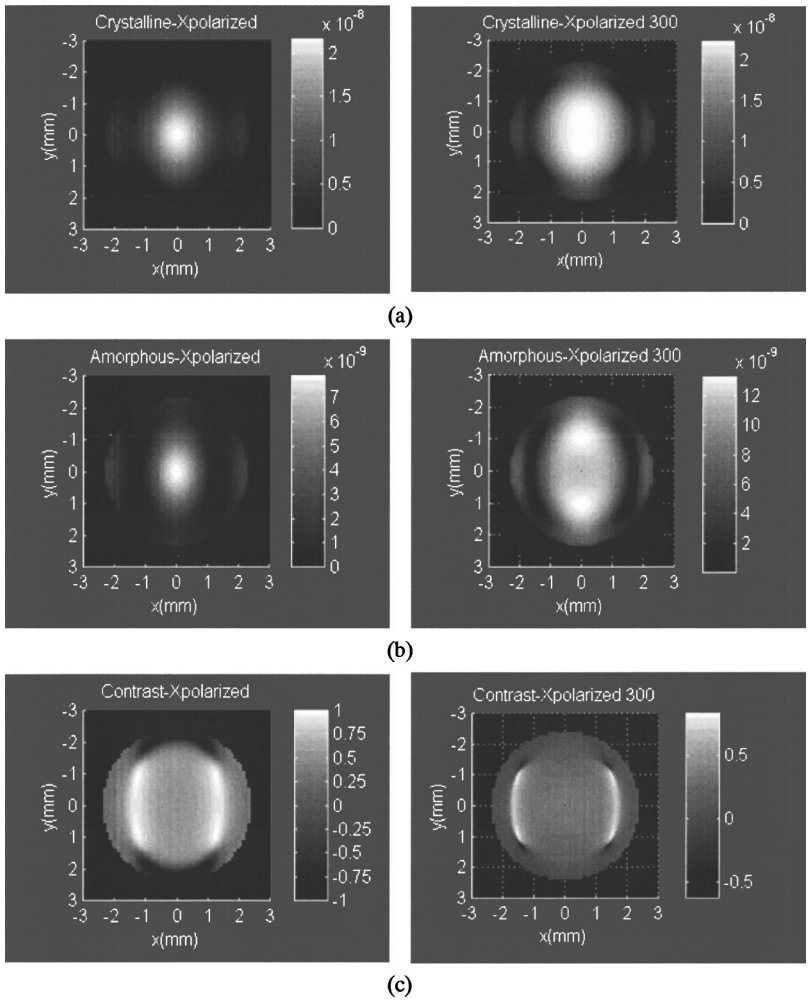

Fig. 3 Intensity distribution of the reflected field in x polarization at the output pupil of the objective (5.2×5.2 mm) for (a) crystalline state (i_X) at 100 nm (left) and 300 nm (right), (b) amorphous state (i_A) at 100 nm (left) and 300 nm (right), and (c) bipolar contrast distribution $(i_X-i_A)/(i_X+i_A)$ with 100 nm (left) and 300 nm (right).

obviously higher than those from depolarized light (y polarized).

Furthermore, we examine the dependence of the air gap on the signal contrast in x and y polarizations. The variations of difference $S_{Xi}-S_{Ai}$ and sum $S_{Xi}+S_{Ai}$ ($i=1, 2$: x, y polarization, respectively) with the gap is shown in Fig. 5(a). The sum of x-polarized intensity $S_{X1}+S_{A1}$ oscillates as the gap width is varied, resulting in the variation of signal contrast. On the other hand, $S_{X2}+S_{A2}$ and $S_{X2}-S_{A2}$ in y polarization are less affected by the gap width.

In general, the signal detection for phase change material does not consider polarization; thus no polarized elements such as PBS are used. For comparison, we also investigated a conventional readout scheme for PC media that use a single beamsplitter and detector to extract reflectance (crystalline and amorphous state) by replacing PBS and individual detectors S_1 and S_2. The signal contrast as a function of gap width is between that of x-and y-polarized detections, and is very closed to x-polarized detection, as shown in Fig. 5(b). The intensity distribution is contributed from both x and y polarizations, and the z component of the collimated beam is insignificant and can be omitted. At 100-nm gap width, for example, the intensity ratio of x to y polarization S_1/S_2 is 6.7 for the crystalline state and 3.9 for the amorphous state, respectively. It is evident that the x components dominate; therefore, signal contrast degradation due to y polarization can be neglected for an $\mathrm{NA}_{\mathrm{eff}}=1.1$ full aperture system. In addition, the gap is considered to be one of the thin-film layers. As the gap width changes, the reflective properties are modified, resulting in the shift of the peak in x polarized from 0-to 50-nm gap width and signal reverse in a y-polarized detection around a gap width of 0 nm.

Then we use an annular aperture to block the rays below the critical total internal reflection (TIR) angle $\theta_c=\sin^{-1}(1/n_{\mathrm{SIL}})$ to concentrate on the impacts of evanescent coupling. With increase of air gap, sum of both x polarized $S_{X1}+S_{A1}$ and y polarized $S_{X2}+S_{A2}$ increase. On the other hand, the signal $S_{X1}-S_{A1}$ is drastically reduced, as shown in Fig. 6(a). In a view of incident plane-wave spectrum, the field amplitude in an air gap without any recording medium

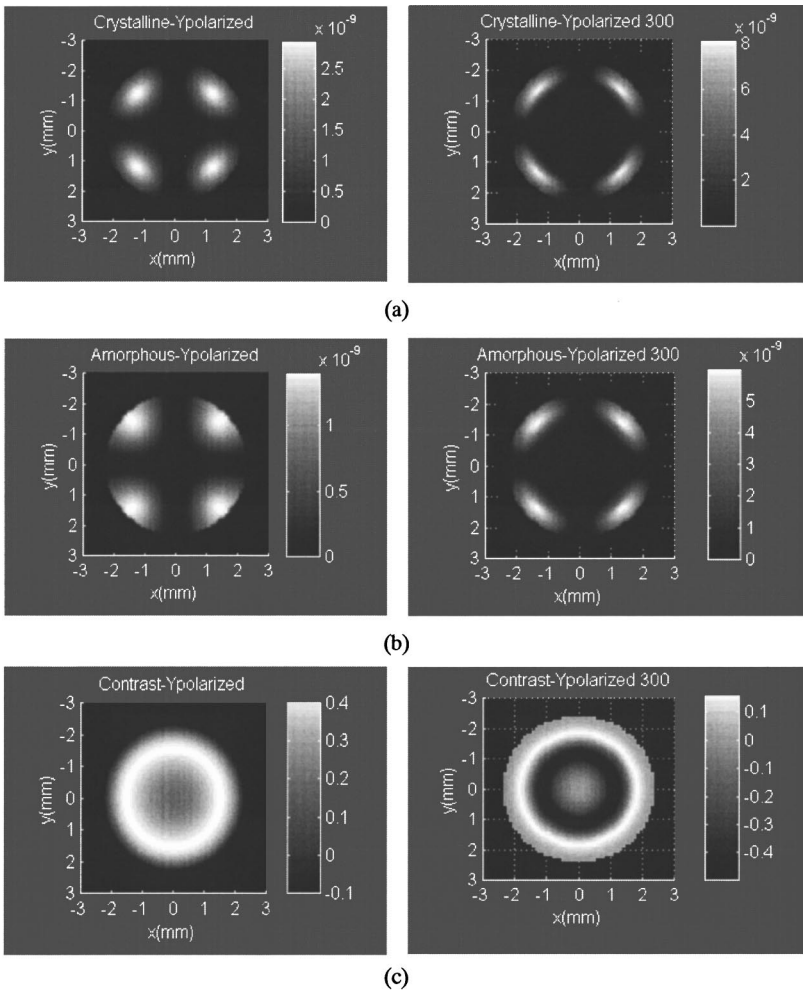

Fig. 4 Intensity distribution of the reflected field in *y* polarization at the output pupil of the objective (5.2×5.2 mm) for: (a) crystalline state (i_X) at 100 nm (left) and 300 nm (right), (b) amorphous state (i_A) at 100 nm (left) and 300 nm (right), and (c) centrally symmetrical contrast distribution $(i_X - i_A)/(i_X + i_A)$ with 100 nm (left) and 300 nm (right).

decays with z (distance from the bottom of the SIL) as $\exp(-\zeta z)$, where decay term

$$\zeta = \frac{2\pi}{\lambda_0} n_{\mathrm{SIL}} (\sigma_X^2 + \sigma_y^2 - 1/n_{\mathrm{SIL}}^2)^{1/2}$$

$$(\sigma_X = \sin\theta\cos\phi, \quad \sigma_y = \cos\theta\cos\phi).$$

As the gap width increases, there is less evanescent wave coupling through to the recording medium for a given angle of the marginal ray $[\mathrm{NA}_{\mathrm{eff}} = n_{\mathrm{SIL}}(\sigma_X)_{\mathrm{MAX}} = n_{\mathrm{SIL}}(\sigma_y)_{\mathrm{MAX}}]$. Thus, a substantial reduction in evanescent coupling causes increase of total reflectance[8,10] and reduction of interaction between the incident beam and recording medium. Compared with full aperture, the signal contrast shown in Fig. 6(b) drops more sharply. At 100-nm gap width, for example, the signal contrast is down to about 75% from its peak in the *x*-polarized detection. If the gap width is larger than 350 nm, the signal contrasts in both polarizations approach zero because incident rays are all reflected and not interacted with multilayer stacks anymore.

A similar analysis was carried out for a higher numerical aperture of $\mathrm{NA}_{\mathrm{eff}} = 1.48$. Compared with the case of $\mathrm{NA}_{\mathrm{eff}} = 1.1$, there is a more apparent discrepancy between *x* and nonpolarized detections in signal contrast versus gap width for the $\mathrm{NA}_{\mathrm{eff}} = 1.48$ system, as shown in Fig. 7. In a conventional detection scheme for PC media, the signal contrast of reflection difference between crystalline and amorphous states is from contributions of both *x* and *y* polarizations. For an *x*-polarized incident beam, the bending of the polarization vectors by a higher NA lens induces, in addition to original polarization along the *x* direction, more sizable components along the *y* direction. Thus the signal degradation due to the *y* polarization is more significant. At a gap width of 100 nm, for example, the reflected intensity ratio of *x* to *y* polarization S_1/S_2 is 4.17 for the crystalline state ($S_1/S_2 = 6.7$ at $\mathrm{NA}_{\mathrm{eff}} = 1.1$), and 2.47 for the amorphous state ($S_1/S_2 = 3.9$ at $\mathrm{NA}_{\mathrm{eff}} = 1.1$), respectively.

In contrast, we also consider typical magnetic optical (MO) media under the SIL readout. For an *x*-polarized in-

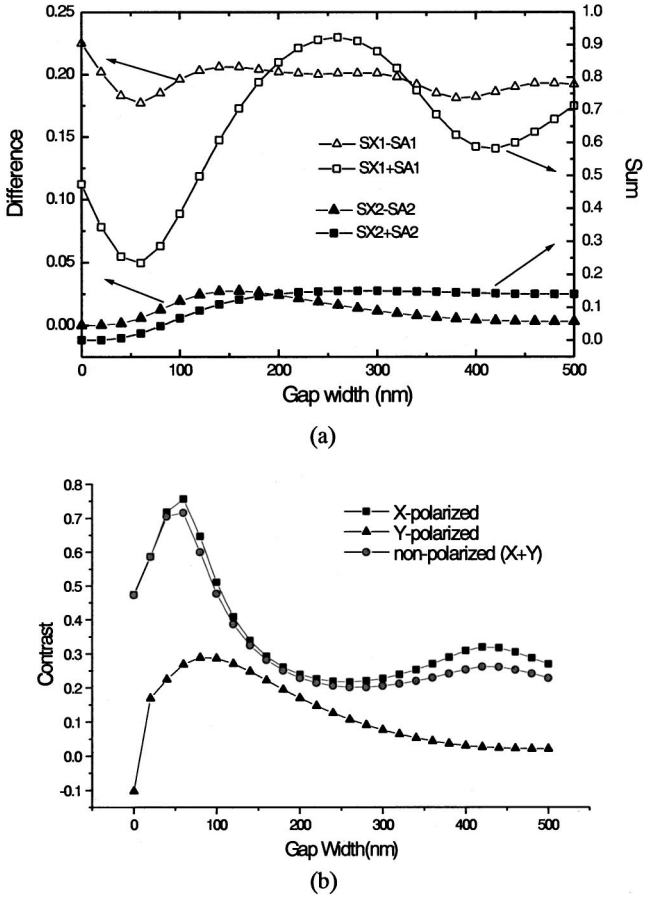

Fig. 5 (a) Reflectance difference between crystalline and amorphous state $S_{Xi}-S_{Ai}$ and sum $S_{Xi}+S_{Ai}$ ($i=1$, 2: *x, y* polarization, respectively) signal level with the gap width for optimized disk structure shown in Fig. 1, with $NA_{eff}=1.1$ full aperture. (b) Signal contrast $(S_{Xi}-S_{Ai})/(S_{Xi}+S_{Ai})$ dependence on gap width in *x, y* polarized and conventional detection for PC media.

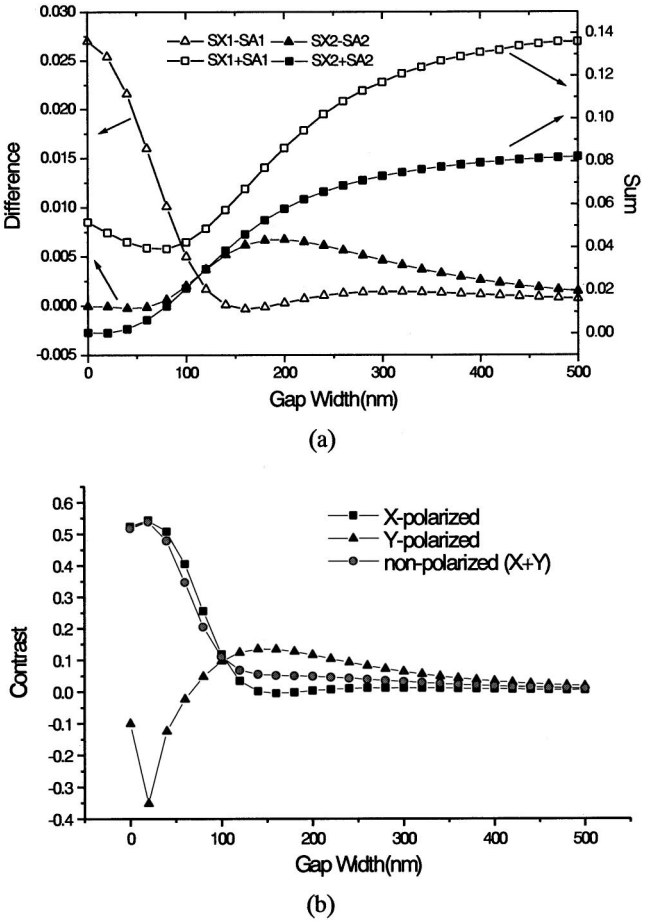

Fig. 6 (a) Reflectance differences between the crystalline and amorphous states $S_{Xi}-S_{Ai}$ and sum $S_{Xi}+S_{Ai}$ ($i=1$, 2: *x, y* polarization, respectively) signal level vary with gap width, with $NA_{eff}=1.1$ annular aperture blocking the rays below the TIR critical angle. (b) Signal contrast $(S_{Xi}-S_{Ai})/(S_{Xi}+S_{Ai})$ dependence on gap width in *x, y* polarized and conventional detection for PC media.

cident beam, the component of *y* polarization contributed by an MO Kerr effect is added on quadrants of nonmagnetic effect. When a balanced differential detector system is used, the nonmagnetic effect is cancelled,[9] thus there is no need to consider the discrepancy between *x*- and *y*-polarized detection in MO. Moreover, for a circularly polarized incident beam on PC media, all the signals from both *x* and *y* polarizations are symmetric, thus there is no discrepancy between *x*- and *y*-polarized detections.

Again we used an $NA_{eff}=1.48$ annular aperture to block the rays below the TIR angle to examine the signal contributed from the evanescent mode. Compared with the $NA_{eff}=1.1$ annular aperture, besides the steeper decrease of the signal contrast, there is no improvement for signal contrast even in small gap width, as shown in Fig. 8, due to the variations of both positive $i_x > i_A$ and negative $i_x < i_A$ reflected intensity within the evanescent ring region, causing the cancellation of signal contributions.

The calculated results show that the detection of SIL systems is from individual contributions of propagating and evanescent modes, respectively. For the case of an SIL coupled to a recording medium through the air gap, standing waves in propagating mode and decay waves in evanescent mode in *x* and *y* polarizations are different. Moreover, signal contrast of *x*-polarized detection is always higher than nonpolarized detection for PC media. Taking the $NA_{eff}=1.48$ full aperture objective for example, the in-

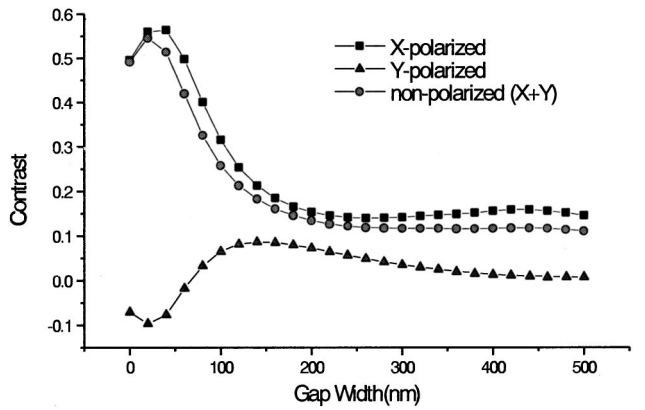

Fig. 7 Signal contrast dependence on gap width for $NA_{eff}=1.48$ full aperture in *x, y* polarized and conventional detection for PC media.

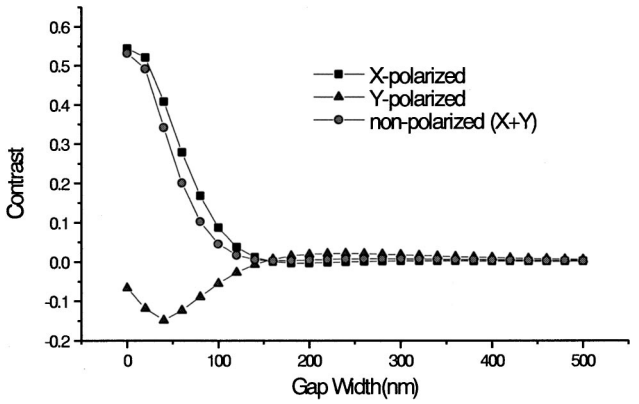

Fig. 8 Signal contrast dependence on gap width for $NA_{eff}=1.48$ annular aperture in *x, y* polarized and conventional detection for PC media.

tensity and contrast ratio of *x*-polarized/nonpolarized detection reveal a trade-off between signal improvement and intensity from the detector, as shown in Fig. 9. The *x*-polarized contrast V_1 is a factor 1.0 to 1.35 higher than nonpolarized detection for conventional PC detection with different gap width, at a cost of less than 25% intensity reduction. Thus, filtering *y*-polarized light and using only *x*-polarized detection are feasible schemes to increase signal contrast, yet at a cost of less than 25% total intensity reduction.

5 Conclusion

The impacts of polarization on the readout signal in an SIL-based system for applications of phase change disk structure were studied. For an *x*-polarized incident beam, the bending of the polarization vectors by a high NA lens results in sizable *y* components as well as original polarization along the *x* direction. Because the reflection coefficients of the thin-film structure are both angle and polarization dependent, the signal contrast was a different function of air gap width for *x* and *y* polarizations. Evanescent coupling in both polarizations drastically affects the readout signal contrast, which sharply reduces with increasing gap width, thus limiting the spacing between SIL and the recording media. For a conventional PC detection scheme, the reflected field is contributed from both *x* and *y* polarizations and the signal contrast is reduced by the depolarized components (*y*-polarized from *x*-polarized incident beam), which becomes more seriously for higher NA systems. A method of filtering *y* polarization and using only *x*-polarized detection results in a factor 1.0 to 1.35 times higher than nonpolarized detection for conventional PC detection at different air gap widths, yet at a small intensity reduction.

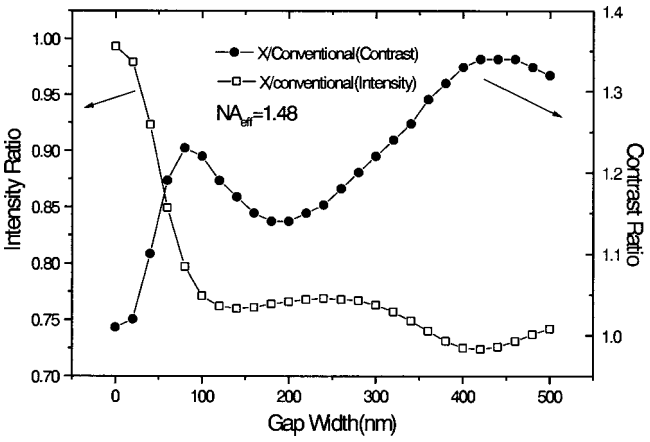

Fig. 9 Intensity and signal contrast ratio of *x*-polarized/nonpolarized detection with $NA_{eff}=1.48$ full aperture system. The *x*-polarized contrast is a factor of 1.0 to 1.35 improvement when the gap width increased, at less than 25% total intensity reduction.

Acknowledgment

This work was supported by the National Science Council of the Republic of China under contract No. NSC 88-2622-L009-002 and ''Photonics Science and Technology for Tera Era'' Center of Excellence under contract No. 89-E-FA06-1-4.

References

1. D. W. Pohl, W. Denk, and M. Lanz, ''Optical stethoscopy image recording with resolution λ/20,'' *Appl. Phys. Lett.* **44**, 651–653 (1984).
2. E. Betzig, J. K. Trautman, R. Wolfe, E. M. Gyorgy, P. L. Finn, M. H. Kryder, and C.-H. Chang, ''Near-field magneto-optics and high density data storage,'' *Appl. Phys. Lett.* **61**, 142–144 (1992).
3. S. Hosaka, T. Shintani, M. Miyamoto, A. Hirotsune, M. Terao, M. Yoshida, K. Fujita, and S. Kammer, ''Nanometer-sized phase-change recording using a scanning near-field optical microscope with a laser diode,'' *Jpn. J. Appl. Phys., Part 1* **35**, 443–447 (1996).
4. S. M. Mansfield, W. R. Studenmund, G. S. Kino, and K. Osato, ''High numerical aperture lens system for optical storage,'' *Opt. Lett.* **18**, 305–307 (1993).
5. B. D. Terris, H. J. Mamin, D. Rugar, W. R. Studenmund, and G. S. Kino, ''Near-field optical data storage using a solid immersion lens,'' *Appl. Phys. Lett.* **65**, 388–390 (1994).
6. I. Ichimura, S. Hayashi, and G. S. Kino, ''High density optical recording using a solid immersion lens,'' *Appl. Opt.* **36**, 4339–4348 (1997).
7. I. Ichimura, K. Osato, F. Maeda, H. Owa, and H. Ooki, ''High density optical disk system using a solid immersion lens,'' *Proc. SPIE* **2514**, 176–181 (1995).
8. S. Hayashi and G. S. Kino, ''Solid immersion lens for optical storage,'' *Proc. SPIE* **2412**, 80–87 (1995).
9. T. D. Milster, J. S. Jo, and K. Hirota, ''Roles of propagating and evanescent waves in solid immersion lens systems,'' *Appl. Opt.* **38**, 5046–5057 (1999).
10. T. D. Milster, J. S. Jo, K. Hitora, K. Shimura, and Y. Zhang, ''The nature of the coupling field in optical data storage using solid immersion lenses,'' *Jpn. J. Appl. Phys., Part 1* **38**, 1793–1794 (1999).
11. Wei-Hung Yeh and M. Mansuripur, ''Evanescent coupling in magneto-optical and phase-change disk systems based on the solid immersion lens,'' *Appl. Opt.* **39**, 302–315 (2000).
12. M. Mansuripur, ''Certain computational aspects of vector diffraction problems,'' *J. Opt. Soc. Am. A* **6**, 786–805 (1989).
13. M. Mansuripur, ''Effects of high-numerical-aperture focusing on the state of polarization in optical and magnetic-optic data storage systems,'' *Appl. Opt.* **30**, 3154–3162 (1991).
14. P. Yeh, *Optical Waves in Layered Media*, Wiley and Sons, New York, (1991).
15. T. D. Milster, K. Shimura, J. S. Jo, and K. Hitora, ''Pupil-plane filtering for improved signal detection in an optical data storage system incorporating a solid immersion lens,'' *Opt. Lett.* **24**, 605–607 (1999).

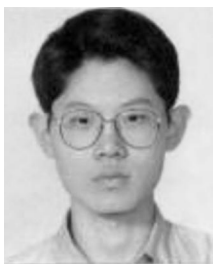

Chung-Hao Tien received the BSc degree in communication-engineering from National Chiao Tung University, Hsinchu, Taiwan, Republic of China, in 1997. He is currently a PhD student in the Institute of Electro-Optical Engineering in National Chiao Tung University. He is working in the field of optical storage, and his main interests are in the analyses of recording and readout characteristics of SIL-based optical systems and microlenses for optical data storage applications.

Yin-Chieh Lai received his PhD degree in electrical engineering from Massachusetts Institute of Technology, USA, in 1991, and became a faculty member at the Institute of Electro-Optical Engineering at National Chiao Tung University, Taiwan, in the same year. He is now a professor there and is conducting research in the area of quantum optics, nonlinear optics, laser physics, optical simulation, and fiber-optic technology.

Han-Ping David Shieh received the BSc degree in physics from National Taiwan University, Taipei, Taiwan, Republic of China, in 1975; the MSc degree in electrical engineering from the Ohio State University, in 1980; and the PhD degree from Carnegie Mellon University, Pittsburgh, PA, in 1987. Since 1988, he has been a research staff member at IBM Research Division, T J Watson Research Center, and Adjunct Assistant Professor of the Department of Electrical and Computer Engineering, Carnegie Mellon University, Pittsburgh, PA. Since 1992, he has been a professor at the Institute of Electro-Optic Engineering and the Microelectronics and Information Research Center, National Chiao Tung University, Hsinchu, Taiwan, Republic of China. He has worked in the field of optical storage for over ten years, and his main interests now are the technologies of optical data storage and flat-panel display.